Permeation Barrier for Lightweight Liquid Hydrogen Tanks

Dissertation zur Erlangung des Doktorgrades
der Mathematisch-Naturwissenschaftlichen Fakultät
der Universität Augsburg

vorgelegt von

Daniel Schultheiß

16. April 2007

Chapter 2

Permeation in Metals and Polymers

"*A theory is something nobody believes, except the person who made it ...*" continued on page 61

This chapter gives a detailed description of permeation in metals and polymers. First, the structure of these materials is explained and fundamental equations to describe gases and their transport are presented. The next two sections deal with sorption and diffusion, the subprocesses of permeation. The permeation process itself is treated afterwards. Finally, the developed program to simulate permeation is presented.

2.1 Structure of Metals and Polymers

The mechanism and the rate of permeation are strongly related to the structure of the bulk material. While metals and metal alloys are characterized by their compact crystal structure, polymers are amorphous.

The three types of crystal structure in metals, face-centered cubic (fcc), body-centered cubic (bcc) and hexagonal close-packed (hcp), are shown in figure 2.1. Table 2.1 summarizes the lattice types and the according lattice constants of selected metals. The structure of a true metal, however, is a crystal containing imperfections. Common defects are vacancy or interstitialcy (point defects), edge or screw dislocation (line defects) and grain boundaries (planar defects).

The common feature of all polymers is the co-existence of molecule chains and free volumes [23–26]. The noncrystalline structures of polymers are less tightly packed than metals. Depending on the cross-linkage of the chains one distinguishes between thermoplastics, thermosets and elastomers. In this thesis, only thermosets and thermoplastics are further considered and illustrated in figure 2.2. Thermoplastics consist of linear or less branched but not cross-linked chains. The bonding between the chains are owing to van-der-Waals or hydrogen-bridge forces. The polymer chains of thermosets, on the contrary,

Table 2.1: Crystal structure of some metals. The lattice constant a is taken from [22].

lattice	metals	a / Å
fcc	copper, silver, gold, platinum, aluminum, nickel, lead, palladium	3.52 – 4.95
bcc	iron, vanadium, niobium, tantalum, molybdenum, tungsten	2.87 – 3.31
hcp	titanium, zinc	2.67 – 2.95

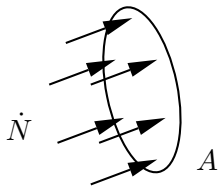

Figure 2.3: Definition of the flux J. The amount of particles dN crosses the area A in time dt.

where s is the pumping speed and p is the pressure at the inlet of the pump. In many applications, the area specific gas flow is used to describe transport processes:

$$q = Q/A, \tag{2.5}$$

where A is the area.

The transport of gases in permeation processes is usually described by the flux, J. The flux is defined as the rate of particles per unit area, see figure 2.3

$$J = \frac{1}{A}\frac{dN}{dt}. \tag{2.6}$$

Substituting (2.2) and (2.3) in (2.6), the relationship between the flux and the gas flow is

$$J = \frac{1}{A\,R\,T}\,Q. \tag{2.7}$$

The flux can also be expressed by the concentration flow. The concentration of a material is defined as the number of particles dN per occupied volume dV:

$$C = \frac{dN}{dV}. \tag{2.8}$$

Substituting (2.8) in (2.6) and considering $dV/dt = A\,dx/dt = A\,v$, where v is the average velocity of the particles, one obtains

$$J = C\,v. \tag{2.9}$$

2.3 Sorption

2.3.1 Modes of Sorption

Sorption is the general term for all interactions at surfaces between molecules of two phases. In this thesis, only the interactions between molecules of the gas phase (solute) and the surface of a solid (solvent) are considered.

If molecules of the gas phase hit the surface of a solid, they can stick on it with a certain probability. This process is called adsorption. Depending on the existing cohesion forces, one defines physisorption (van-der-Waals forces) and chemisorption (covalent bond forces). The molar sorption energy of physisorption and chemisorption are approximately

30 kJ/mol and 500 kJ/mol, respectively [30; 31]. Desorption is the opposite process of adsorption. Absorption denotes the migration of the solutes into the bulk of the solvent.

Adsorption can be classified into mono-layer and multi-layer adsorption. Mono-layer adsorption is typically described by the Langmuir model [32]. There, only one layer of gas atoms/molecules can stick on the surface of the solvent. The coverage grade, θ, is defined for values between 0 (no adsorbed atoms) and 1 (surface is totally covered by one layer of solutes). Additionally, Langmuir presumed that the solutes do no react with each other. Hence, the adsorption rate or the sticking probability, respectively, is proportional to $1 - \theta$. The desorption rate is proportional to $\theta \exp[-E_a/RT]$. The Boltzmann factor, $\exp[-E_a/RT]$, is typical for thermally activated process. It expresses the probability of one atom or molecule accumulating the additional energy E_a to overcome a barrier [33]. In equilibrium of adsorption and desorption, the according rates are equal and one obtains the Langmuir isotherm

$$\theta = \frac{B\,p}{1 + B\,p}, \tag{2.10}$$

where θ is the surface coverage factor, $B = B_0 \exp[-E_B/RT]$ is a temperature-dependent material constant reflecting the bond strength of the solute, and p is the pressure in the gas phase.

Multi-layer adsorption reflects the ability of solutes to stick on already adsorbed solute layers. While mono-layers are physisorbed or chemisorbed, the following layers are condensed gases [30]. Brauner, Emmett and Teller (BET) have developed a model to describe this process. They presumed, that the next layer can only grow if the underlying layer is fully covered. Hence, the adsorption rate is again proportional to $1 - \theta$. The desorption process follows the laws of evaporation. The derived surface coverage factor is described by the BET isotherm [30]

$$\theta = \frac{r_{\mathrm{BET}}\,p}{(p_s - p)\,[1 + (r_{\mathrm{BET}} - 1)\,p/p_s]}, \tag{2.11}$$

where r_{BET} is the ratio of the sticking times of adsorption and condensation layer, p is the gas pressure, p_s is the vapor saturation pressure.

Considering $\theta \propto C$, the Langmuir isotherm (2.10) and the BET isotherm (2.11) can be modified respectively to

$$C = \frac{S^* B\,p}{1 + B\,p} \text{ and } C = \frac{S^{**}\,r_{\mathrm{BET}}\,p}{(p_s - p)\,[1 + (r_{\mathrm{BET}} - 1)\,p/p_s]}, \tag{2.12}$$

where S^* and S^{**} are material constants. Both isotherms describe the dependency of the surface concentration on the pressure at a constant temperature. The functions are schematically plotted in figure 2.4-b and -d, respectively. The Langmuir isotherm approaches a horizontal asymptote for $p \to \infty$. Similarly to the Langmuir-isotherm, the BET isotherm first converges a saturation region. Near the vapor saturation pressure, the concentration becomes infinity.

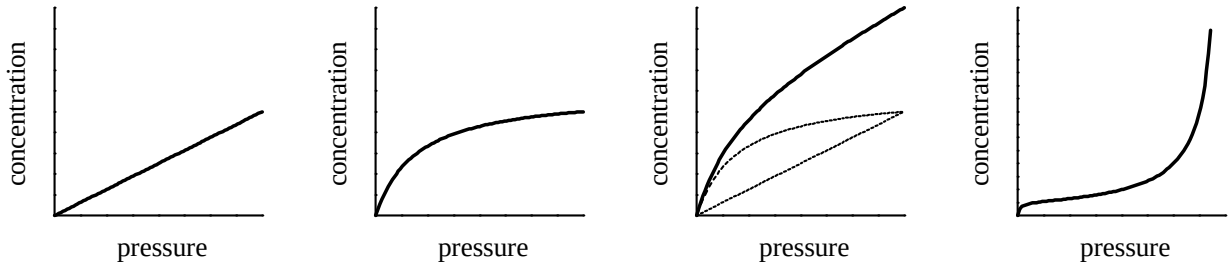

(a) Henry mode (b) Langmuir mode (c) Dual mode (d) BET mode

Figure 2.4: Sorption modes

In both models describing the mono-layer and the multi-layer adsorption, the concentration is direct proportional to the gas pressure for $p \to 0$. This behavior is expressed by Henry's law:

$$C = S\,p, \tag{2.13}$$

where S is called solubility or Henry's constant. The Henry sorption mode is plotted in figure 2.4-a. The solubility includes the probability term for thermally activated processes and is mathematically expressed by the Arrhenius equation

$$S = S_0\,\mathrm{e}^{-E_\mathrm{S}/RT}, \tag{2.14}$$

where S_0 is a temperature-independent but gas-dependent material constant, and E_S is the activation energy of sorption.

The combination of the Henry and Langmuir isotherms is called Dual mode (see figure 2.4-c). Its importance is described in 2.3.3.

2.3.2 Sorption in Metals

The adsorption of gases on metal surfaces can be physisorption or chemisorption. According to Fromm [31], chemisorption is particularly present at active centers on the surface like defects, grain boundaries, corners and edges. In general, the activities of the centers can vary, i. e. the surface is energetically heterogeneous. Depending on the gas type, the adsorption process exhibits different behaviors. In particular, a difference is observed between one and two-atomic gases.

Several publications [31; 34–37] describe the absorption process of two-atomic gases like hydrogen. The molecules first adsorb physically on the surface. The molecules dissociate in a second step and become chemically adsorbed. The adsorbed gas atoms exchange their surface place with the first interstitial layers within the solid (absorption). These reaction steps always exist in both directions, i. e. molecular adsorption counteracts desorption, surface dissociation counteracts recombination. The sum of the reaction steps lead to Sievert's law

$$C = S_\mathrm{S}\,\sqrt{p}, \tag{2.15}$$

where S_S is the solubility of the dissociative absorption or Sievert's constant.

The absorption process of one-atomic gases like helium in metals is rarely investigated. The process is treated as a sequence of physisorption and movement from the surface to interstitial or vacancy sites within the solid [31]. The relationship between surface concentration and gas pressure is commonly modeled by Henry's law (2.13).

Equations (2.13) and (2.15) are valid as long as gases can be considered to be ideal and to follow equation (2.2). At high pressures and low temperatures, gases show a non-ideal behavior. There, the pressure must be substituted by the fugacity, f [25; 26]. A simple form of the fugacity is derived from the Abel-Noble equation of state [38–40]

$$f = p \exp\left(\frac{p\,b}{R\,T}\right),$$

where b is the co-volume. In light of the feasible state limits[1] in this work, the relative error when using p instead of f is less than 2 %. SanMarchi et al. state that the real gas behavior must only be considered at pressures greater than 150 bar [39].

2.3.3 Sorption in Polymers

The absorption process in polymers is independent from the gas type, although the absorption rate varies with the size of the solute. Contrary to metals, two-atomic gases do not dissociate on the surface.

The surface of glassy amorphous polymers ($T < T_G$) can be modeled by a perfect surface coexisting with holes [23; 40; 41]. Elliott [41] explains the existence of the holes with free volume that is frozen into the structure at the glass transition. This surface type is modeled by the Dual sorption mode. While Henry's law (2.13) represents the perfect surface, holes are modeled by the Langmuir isotherm (2.12):

$$C = S\,p + \frac{S^*B\,p}{1 + B\,p}$$

The concentration is direct proportional to p, for $p \to 0$, as depicted in figure 2.4-c. In this case, the Dual mode can be replaced by Henry's law. In the majority of the reviewed publications about permeation in polymers, Henry's law is employed. In these publications, the gas pressure was near the ambient pressure. Raffaelli [24] even found that the H_2 solubility in CFRP at $T = 77\,\mathrm{K}$ and $T = 295\,\mathrm{K}$ is constant for $p = 0 \ldots 11\,\mathrm{bar}$.

Although this work does not investigate the permeation in rubbery polymers ($T > T_G$), the absorption mode is reviewed for completeness. The absorption of gas molecules is mostly described by the BET isotherm (2.11) or the derived Flory-Huggins-Theory [40; 42]. Again, a direct proportionality between the surface concentration and the applied pressure can be observed for low pressures.

[1] The two considered states are ($p = 8\,\mathrm{bar}$, $T = 295\,\mathrm{K}$) and ($p = 2\,\mathrm{bar}$, $T = 20\,\mathrm{K}$). The co-volume of hydrogen is $b = 15.5\,\mathrm{cm}^3/\mathrm{mol}$ [38].

were reported [21; 31; 49; 51–53]. Fromm [31] even stated that only the interstitial site diffusion must be considered. Wipf [51] agreed that hydrogen is mainly existing as an interstitial in metals, but he emphasized the importance of traps in the crystal. The traps are formed by lattice defects like vacancies or dislocations. In general, the traps reduce the diffusivity. Young and Scully [52] investigated the hydrogen diffusion and trapping in high purity aluminum. They observed three distinct diffusion mechanisms with the activation energies 15, 44, and 85 kJ/mol. These diffusion mechanisms are associated with interstitial lattice sites, dislocations, and vacancies, respectively.

The diffusion of inert gases like helium in metals are rarely investigated. Hanika [28] stated that inert gases diffuse extremely badly through metals. Borg and Dienes [49] reviewed the helium diffusion in metals like nickel, gold, aluminum, tungsten and molybdenum. They found that at elevated temperatures the activation energies are much higher than expected for interstitial diffusion. Hence, they concluded that He is predominantly present as a substitutional atom. Borg and Dienes ruled out the vacancy mechanism and stated that helium diffusion follows the dissociative mechanism. Adams and Wolfer [54] investigated the diffusion of helium in nickel. Reviewing measurements and comparing them with their calculations, they concluded that helium primarily exists in substitutional sites. From there, helium may diffuse by interstitial, vacancy or dissociative mechanism. The according activation energies are 52, 126 and 243 kJ/mol, respectively.

The jump frequency of the solute atoms in interstitial sites is the highest compared to other diffusion mechanisms like vacancy and dissociative diffusion. This implies a rapid diffusion process, respectively high diffusivities [49; 55].

2.4.3 Solution of Fick's Laws

The two laws of Fick describing diffusion in a homogeneous material, (2.19) and (2.20), are analytically solved for the one-dimensional diffusion in a membrane.

Let there be a homogeneous membrane with area A and thickness l, where $l \ll \sqrt{A}$. Hence, the diffusion process can be considered as one-dimensional and Fick's laws derive to

$$J = -D\,\frac{\partial C}{\partial x} \quad \text{and} \quad \frac{\partial C}{\partial t} = D\,\frac{\partial^2 C}{\partial x^2},$$

where x is the coordinate in thickness direction. The concentration at the feed side, $x = 0$, and permeate side, $x = l$, may be termed C_f and C_p, respectively. Initially, the concentration is zero throughout the material: $C(x, t < 0) = 0$. At $t = 0$, a constant concentration is applied at the feed side: $C_\mathrm{f}(t \geq 0) = C_\mathrm{f}^0$. Owing to this change of charge, a flow from the feed side to the permeate side starts and C_p changes with time. Crank [56] calculated the flux at the permeate side, if $C_\mathrm{p} \approx 0$ and $C_\mathrm{p} \ll C_\mathrm{f}$ for all t:

$$J(t) = \frac{D\,C_\mathrm{f}^0}{l}\left[1 + 2\sum_{n=1}^{\infty}(-1)^n\,\exp\frac{-D\,n^2\,\pi^2}{l^2}\,t\right]. \tag{2.23}$$

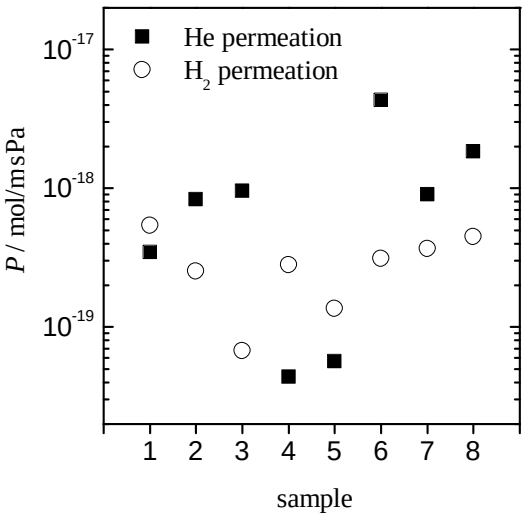

Figure 2.15: Comparison of helium and hydrogen permeabilities of CFRP from [86]. Each sample was tested at room temperature with hydrogen and helium. Although the permeabilities vary strongly, in most cases the helium permeability is greater than the hydrogen permeability.

2.5.5 Comparison of Hydrogen and Helium Permeation

The measurement of hydrogen permeation is often substituted by helium or argon as test gas for reasons of convenience [86–88]. This section gives a comparison of the H_2 and He permeation in polymers and metals.

Considering polymers, the permeability, being a product of D and S (2.33), is mainly dependent on the gas size [41; 46]. While the diffusivity decreases with the penetrant's size, the solubility generally increases with the gas size [41]. Humpenöder [88] reports an exponential dependency of the gas radius on the diffusivity:

$$D_{\text{gas 1}}/D_{\text{gas 2}} = \exp(r_{\text{gas 2}}/r_{\text{gas 1}}).$$

Regarding size and mass, helium is the most similar gas to molecular hydrogen. The van-der-Waals molecular diameter of hydrogen and helium are 276 pm and 266 pm, respectively [89]. With the assumption of Humpenöder above, the diffusivities of hydrogen and helium should have a ratio of $D_{\text{He}}/D_{\text{H}_2} = 2.8$. Humpenöder found in experiments with HDPE, PVC, PC and PA that the He diffusivity is 1.6 – 6.6 times greater then that of H_2.

Measured helium permeabilities in polymers are reported to be comparable to or slightly greater than those of hydrogen. Humpenöder [88], though the diffusivities varied, found similar permeabilities in the considered materials. Goetz et al. [86] investigated the permeation through eight CFRP (IM7/977-2) samples. The results are presented in figure 2.15. Averaging the data, helium permeates slightly stronger than hydrogen. The transport properties of ECTFE, LDPE, PP and PVC are reported in [48; 89–95]. The differences between He and H_2 are minor, though He exhibits a slightly greater permeability. O'Hanlon [96] reviewed the permeabilities of six polymeric materials. He concluded that the helium permeability is greater or equal the hydrogen permeability.

Considering diffusion through metals, hydrogen and helium exhibit different mechanisms, see 2.4.2. Few researches were carried out on the direct comparison of He and H_2

permeation in metals. Schefer et al. [38] stated qualitatively that the helium diffusivity is several orders of magnitude lower than that of hydrogen. McCool and Lin [97] reported a H_2/He selectivity at 573 K for Pd-Ag membranes in the range of 23 to 4770. Collins and Turnbull [98] investigated the permeation of helium and hydrogen through 0.25 mm thick tubes at 1023 K. Hydrogen permeation was detected through Monel, 304 stainless steel, Kovar, Inconel, nickel, and 52 Alloy ($Fe_{50}Ni_{50}$) even at temperatures approaching room temperature. The same metals were not permeated by helium at temperatures as high as 1123 K.

Experiments to directly compare He and H_2 permeation in grain boundaries have not been performed. However, it can be assumed that the permeation behavior of He and H_2 in grain boundaries is similar, when considering that primarily a vacancy motion is present, refer to 2.4.4.

Summarizing, helium and hydrogen exhibit comparable diffusivities and permeabilities in plastics and presumably in metals with grain boundaries. In metals, the permeability of hydrogen is much greater than that of helium.

2.6 Simulation of Permeation

The Fick curve (2.27) describes one-dimensional transient diffusion or permeation, respectively, in homogeneous membranes. However, this equation may not be employed in multi-layer permeation, grain boundary diffusion or permeation through substrates with defective liners. Hence, presuming inhomogeneous materials in general, the measured flux-time curves can differ from the Fick curve.

The reviewed simulations of grain boundary diffusion in 2.4.4 and permeation through defectively coated membranes in 2.5.4 only cover the stationary state. The only transient consideration — of Hwang and Baluffi — may only be used in Harrison type C grain boundary diffusion.

In order to understand the reason for diversely measured $J(t)$ curves in this work though, own transient simulations are carried out. The developed model covers the diffusion in two dimensions. Considering the sorption equation (2.16), this model also allows to simulate two-dimensional permeation. Various materials with different transport properties (D and S) and arbitrary geometries can be defined. Additionally, this model can take the dissociation of molecules into account. The physical assumptions underlying the used model and their mathematical implementation into a program are described in the following.

Definition of the Diffusion Problem

The diffusion problem in one material is described by the two laws of Fick. Considering a body of different materials, Fick's laws may only be applied to each material separately. Knowing the interface conditions, the overall system is determined and can be solved. In the following, the term *phase* is used for a continuous region of one material.

Chapter 7

Conclusions

"*Basic research is like shooting an arrow into the air and, where it lands, painting a target.*" Homer Burton Adkins

Summary

The objective of this thesis was to find an appropriate liner for the inner shell of an LH_2 tank made of CFRP. The liner — located at the outside surface of the shell — is required to prevent permeation of hydrogen through and outgassing from the inner tank into the insulating vacuum. Although outgassing was taken into account, too, the main objective was the permeation measurement of various liner types.

Surveying the outgassing rates and permeabilities from literature, only few metals and glasses satisfy the high requirements for the liners to enable a stable vacuum. Possible production processes to apply those materials on CFRP were studied and evaluated. The maximum allowable temperature of CFRP ($\approx 120 \ldots 140\,°C$) and the applicability on the large and from-adapted structure of the LH_2 tank restricted the number of feasible processes. The chosen liner materials and production processes were

- Foils/sheets: Al, Cu, Sn and SS
- Metal platings with cNiP starting layer: Al, Au, Cu, Sn, and Ni
- Metal platings with cCu starting layer: Cu, Au and Sn
- Thermal spray Al
- PVD: C (DLC) and Ni.

All material tests and investigations were performed on flat specimens (plates, discs). Except for sheets and some of the foils, all liners were applied on CFRP substrates.

Besides permeation tests, the investigation of the various liners included the characterization by means of SEM, thermal shock experiments and adhesive strength tests. The permeation measurements were performed in two separate apparatuses, working between 293 K and 373 K (RTPMA) and between 20 K and 293 K (CPMA), respectively. Both apparatuses were designed and built to investigate CFRP, metals or the combination of both. The transmission method was used to imitate the real load case of the tank as good as possible. Feeding the test gas at one side of the specimen, the molecules permeate through the membrane into a flowing stream. There, the partial pressure of the permeating

gas was measured by means of a mass spectrometer and subsequently converted into the corresponding permeation rate.

The relationship between measured pressure and permeation flux was found by calibrating the mass spectrometer instead of using the constant pumping speed. The acquired calibration factors varied statistically around a mean value. Considering long terms, the mean value increased gradually by time. This increase was found to originate from a degradation of the filaments. Within one year, the sensitivity of the mass spectrometer decreased by factor 10. Hence, an error of 1000 % or more is possible if the speed of the turbomolecular pump is used instead of a calibration factor.

A typical permeation test consisted of the assembly of the specimen, the permeation measurement and the disassembly. During the assembly, an indium wire was squeezed between the specimen and two specimen holders to enable a leak-free sealing. This process was very critical and could not be successfully performed for every specimen. Mainly a rough surface of the specimen or mechanically weak liners were reasons for failing seals. After the subsequent bake-out at approximately 120 °C for 24 hours, the calibration was carried out. The actual permeation measurements were started at room temperature. Depending on the material, the steady-state permeation flux was typically reached after one or two days — if permeation was measurable at all. The change in temperature resulted in a change of the flux approaching a new steady-state within few hours. In very few cases, leaks in the sealing occurred during the change of the temperature.

Initial permeation tests were carried out to prove the functionality and reliability of both apparatuses. The measurements on CFRP and PVC showed consistent results at the RTPMA and CPMA. The permeabilities agreed well with those from the literature. The initial tests also revealed disadvantages of hydrogen as a test gas. The minimum detectable signal of hydrogen was almost four orders of magnitude higher than that of helium. Furthermore, hydrogen permeation was strongly influenced by environmental factors like the daily sunshine durance or the temperature. It is believed that the adsorption and release of hydrogen in the stainless steel chambers is very sensitive to the temperature and causes errors in the measurement. Because the permeabilities of helium and hydrogen were found to be similar in seven specimens, helium was used as test gas in the following.

Important for the quality of the measurement results is the minimum detectable gas flow. The minimum detectable gas flow is the product of the minimum detectable pressure and the calibration factor. Both factors can vary from one experiment to the other, depending on the material of the specimen, the quality of the sealing, and the state of the mass spectrometer's filaments. The typical limit of the detectable He gas flow was between $4 \cdot 10^{-11}$ and $5 \cdot 10^{-10}$ mbar l/s. Related to the permeating area of the RTPMA specimens, the minimum detectable area-specific gas flow was between $1 \cdot 10^{-8}$ and $1.2 \cdot 10^{-7}$ mbar l/s m^2. In order to prove the requirement of the maximum allowable area-specific permeation gas flow through the tank vessel at room temperature (3.3), $q < 1.5 \cdot 10^{-10}$ mbar l/s m^2, the sensibility of the measuring apparatus would have to be between 66 and 800 times better. Hence, the employed measurement apparatuses enabled a comparison of the single liners and a general qualification/feasibility of them. In order to quantitatively prove the requirements, tests on specimens as large as the tank are necessary. On the other hand,

considering the best minimum detectable signal ($1 \cdot 10^{-8}$ mbar l/s m^2) ever measured, a tank vacuum stability time at room temperature of more than 56 days is feasible to prove.

Evaluating the results of the permeation measurements together with those of the adhesive strength and thermal shock tests, the foil/sheet liners and metal platings exhibited the highest potentials. Still, both liner types face some to-be solved challenges.

The structure of foils and sheets was compact and defect-free, which is characteristic for the production process (rolling, extrusion). The adhesive strength of some foils on CFRP was too low which resulted in a partial peeling. With the exception of tin specimens, the permeation gas flow through foils and sheets was lower than the detection limit. Remarkably, a 25 µm Cu foil adhered on CFRP and three welded, 1 mm thick Al sheets did not allow any measurable permeation. Considering the 25 µm Cu foil, the permeation flux through the protected CFRP was reduced at least by factor 7400 compared to CFRP. The measured He permeability of copper was less than $2 \cdot 10^{-22}$ mol/m s Pa. Introducing sheets or foils as a liner on a free-form CFRP inner tank, the application of them would require a leak-free joining method with low heat production. This issue was not investigated in this thesis.

In contrast to foils, full metal platings can be produced on the outside of an inner LH_2 tank vessel. The investigated metal platings consisted of at least two layers. The first layer was produced by chemical deposition of copper or nickel. The typical thickness of this initial layer was between 1 and 10 µm. Subsequently, the functional layer was applied by either chemical or electrochemical deposition. The materials of the functional layers were copper, nickel, gold, tin and aluminum. Depending on the material and the process parameters, the coatings contained grain-like structures on the surface. While the diameter of these grain-like structures was only 1 – 3 µm for chemical copper, those of aluminum were up to 160 µm in diameter. The coatings consisting of chemical nickel contained cracks which can be explained by their brittleness. Tin coatings were fully traversed by cracks after thermal shock which was ascribed to the phase transition at 286 K. The gold layers, having a thickness of only few micrometers, were not fully deposited but contained holes. The aluminum liners either exhibited uncoated spots or channels. Some of the metal platings, independent from the material and thickness, were characterized by circular holes. These holes, being maximal 100 µm in diameter, originated from defects (voids, caverns) on the surface of the substrate. The caverns on the CFRP surface were only coated by material few micrometers thick or not at all. The existence of holes had a substantial impact on the measured permeabilities. Functional liners made of nickel sulfamate or copper containing no holes were impermeable within the accuracy of the measurements. In this case, the permeation gas flow through CFRP was reduced by more than factor 7400 (S46c, S65). On the contrary, a copper coating with nine holes (S10) reduced the permeation flux through CFRP only by factor 67. It was shown that — independent from the coating material — the total permeability is approximately proportional to the number of holes.

Temperature-dependent permeation measurements on metal-plated and uncoated CFRP specimens were performed between 20 K and 373 K. The measured permeation flux generally decreased with decreasing temperature. For temperatures below approximately 200 K,

no permeation could be detected in all investigated specimens. In particular, no permeation gas flow could be measured at 20 K. The extrapolated permeability of uncoated CFRP (worst case) at 20 K is $5 \cdot 10^{-62}$ mol/m s Pa.

In some specimens containing either a cNiP, cNiP-cAu or cNiP-Sn coating, sudden and short increases of the permeation flux were recorded during the cooling phase. The subsequent measurement at RT revealed an increase of the permeation rate to values of uncoated CFRP. Hence, the peaks of the flux resulted from the formation of cracks in the according liners. Specimens with a copper or nickel functional layer did not show any peaks and did not form microcracks during cooling.

The measured activation energies of permeation through metal-plated CFRP were between 7 and 20 kJ/mol, but mostly below 15 kJ/mol. These activation energies are lower than those of uncoated CFRP (18 ± 1 kJ/mol). Simulations and calculations proved, that this behavior only occurs if the activation energy of permeation through the liner is low. Permeation though CFRP with an impermeable but defective coating would result in the same activation energy as uncoated CFRP. The low activation energy of the coating is assumed to be caused by grain boundary diffusion.

The assumption of grain boundary diffusion is emphasized by transient simulations performed with a self-written `Matlab` program. The aim of the simulations was to understand the various existing flux-time curves obtained from the experiments. In particular, some measured $j(\tau)$ curves showed strong deviations from the Fickian curve, which describes permeation through a homogeneous material. Three models were employed: grain boundary diffusion, permeation through two homogeneous layers and permeation through a substrate with a defective liner. The parameters of the simulations were chosen to reflect the experiments as good as possible. Neither the simulation of two-layer permeation nor those of permeation through defectively coated CFRP could reproduce the $j(\tau)$ curves found in the experiments. On the contrary, the simulation of grain boundary diffusion could describe the $j(\tau)$ shape obtained from the experiments. It was found that the deviations from the Fickian curve depend on the size of the boundaries, the distance between those and the ratio between the grain and grain boundary diffusivity.

Considering the scattering in the values of the permeabilities, the low activation energies, and the partly found strong deviations of the $j(\tau)$ curve from the Fickian curve, the permeation through metal-plated CFRP specimens can be described as followed: A closed, defect-free metal plating is impermeable for helium. If defects in the coating or very low coating thicknesses exist, then the barrier function of the coating is reduced. The permeation through these coating defects with low thickness is dominated by grain boundary diffusion. The existence of grain boundaries additionally justifies the usage of helium instead of hydrogen. In grain boundaries, vacancy diffusion is assumed to be present and results in a similar diffusion behavior of He and H_2.

Besides sheets/foils and metal platings, thermal spray aluminum and physical vapor deposited carbon and nickel coatings were investigated. The three latter coatings did not reduce the permeation flux dramatically. While the PVD Ni and the DLC coatings contained cracks presumably owing to high internal stresses, the thermally sprayed Al coating did not form a closed layer.

Evaluating and comparing the permeation properties, sheets/foils and defect-free metal platings enabled a reduction of the permeation flux through CFRP below the minimum detection limit. Using this detection limit to calculate the stability time of the insulating tank vacuum, only a lower limit of the time can be given. At room temperature, a 30 µm Al foil, a 25 µm Cu foil or a 100 µm Cu metal plating would enable a vacuum stability for at least 2 days. An aluminum sheet with 1 mm in thickness would even increase the minimum expectable time to 9 days. At 20 K, no reasonable permeation is expected.

The results of this work were used to choose an appropriate liner for the CFRP inner tank introduced in chapter 1. Considering and evaluating all properties of the various liners, the CFRP tank was coated by means of metal plating (see figure of the title page). The coating consisted of a chemical copper layer, followed by an electrochemical copper layer. Although the tank was fully coated, permeation tests could not be performed owing to predominating leaks in the CFRP structure.

Summarizing, a promising liner material and the according production process were found to prevent permeation through CFRP at temperatures between 20 and 373 K. The final qualification of this liner, however, must be performed on a tank itself.

Future Work

This work has shown that metallic liners are feasible to apply on CFRP and to reduce the permeation rate below the detection limit. Still, there is a lot of space for improvements and future work.

The minimum detection limit of the measurements was too high to present results that can prove the tank requirements for the vacuum stability. An improvement can be achieved by either using larger specimens or applying higher feed pressures. When increasing the feed pressure, the limited ultimate strength of the specimens and the sensitivity of the sealing must be considered. Larger specimens are more difficult to seal, especially when measuring at varying temperatures. The lower stiffness and strength of larger specimens must also be taken into account. The usage of tubes instead of flat specimens would be an alternative. A promising approach to enhance the sensitivity of the mass spectrometer is given by Firpo and Pozzo [153]. There, the pumping speed of the gas of interest is reduced, while all other gases are evacuated constantly. Employing this method, the minimum detectable signal could be reduced by factor 10.

It was shown, that electroplatings on CFRP can be a permeation barrier if they do not contain defects. This implies that the surface of the CFRP must be free of caverns. Studies on the CFRP production process could indicate and subsequently prevent factors that favor the formation of those caverns. A promising approach is the usage of the resin transfer molding (RTM) process instead of the VARI process. In the RTM process, air enclosures are more present within the CFRP but less near the surface [154]. At the end of this work, four $200 \times 100\,\mathrm{mm}^2$ CFRP plates were produced by means of RTM and subsequently coated by 50 µm copper. Only one hole was found in the four liners having an area of $800\,\mathrm{cm}^2$. Additionally to the improvement of the CFRP surface, the coating process can

be further investigated. Emphasis should be laid on understanding why caverns cannot be fully coated with increasing liner thickness.

All tests were performed on flat, nearly perfect specimens. However, the produced free-form CFRP tank contained leaks which were probably formed owing to different load cases and/or imperfections in the CFRP. Presuming an always existing potential of leakage in the CFRP structure, the size of the cracks causing this leakage should be determined. Subsequently, the ability to cover these cracks by coating should be investigated. Another option is a liner consisting of two layers. The first layer is very ductile, insensitive to thermal shocks or mechanical loads, and does not form cracks. Hence, this layer shall work as a crack stopper and prevent leakage. The second layer consists of a liner presented in this work and prevents permeation and outgassing.

Foils showed a great potential as a permeation barrier. However, leak-free joining methods must be found to employ foils as a liner. Processes like welding (high temperatures) or adhering (leakage) are not feasible. An alternative solution would be the application of single foil parts and the subsequent coating of the joining lines.

The qualification of the liners also requires the measurement of their outgassing rates. In order to be able to prove very low outgassing rates, large specimens — preferably the tank itself — should be used. The influence of the bake-out temperature and bake-out time can be determined by sensitivity studies. Cleaning methods, like chemical or glow discharge cleaning, should be investigated to further reduce the outgassing rate.